IEEE Access
Multidisciplinary ⋮ Rapid Review ⋮ Open Access Journal

Received 18 August 2025, accepted 29 September 2025, date of publication 6 October 2025, date of current version 13 October 2025.

Digital Object Identifier 10.1109/ACCESS.2025.3618406

RESEARCH ARTICLE

Large Side Hole Polymer Optical Fiber-Based Surface Plasmon Resonance Sensor

JITENDRA NARAYAN DASH[1], CHENG XIN[2], AND HWA-YAW TAM[2], (Life Fellow, IEEE)
[1]Division of Physics, School of Advanced Sciences, Vellore Institute of Technology, Chennai, Tamil Nadu 600127, India
[2]Photonics Research Institute, Department of Electrical and Electronic Engineering, The Hong Kong Polytechnic University, Hong Kong, SAR, China
Corresponding author: Jitendra Narayan Dash (jitendranarayan.dash@vit.ac.in)

ABSTRACT A ZEONEX-based large side air hole polymer optical fiber (LSAHPOF) is proposed and numerically analyzed for surface plasmon resonance (SPR)-based sensing applications. The fiber has been successfully fabricated using a drawing tower facility and the fabrication process is designed such that the fiber core is fully exposed to the side air hole, enabling direct metal deposition onto the core surface. Gold has been considered as the plasmonic metal for the numerical analysis. The low optical loss of ZEONEX in the visible wavelength region, combined with the surface plasmon resonance (SPR) frequency of gold occurring in the same spectral range, makes ZEONEX an excellent material choice for SPR-based sensing applications. On the other hand, the humidity insensitivity of ZEONEX makes it well-suited for sensing applications in aqueous environments. The presence of a large side hole facilitates efficient metal coating and easy introduction/removal of the analyte, without adversely affecting the sensor's performance, even with increased hole size. The sensor's performance has been numerically evaluated for RI of analytes as well as for detecting thickness of biolayer. The analysis reveals a maximum wavelength sensitivity of 3500 nm/RIU and a high resolution of 2.8×10^{-5} RIU and an amplitude sensitivity of 696 RIU^{-1}. On the other hand, the sensitivity for thickness of biolayer has been found to be 1.54 with a maximum resolution of 64 pm.

INDEX TERMS Polymer optical fiber, side hole, sensor, surface plasmon resonance, ZEONEX.

I. INTRODUCTION

Surface plasmon resonance (SPR)-based sensors have been extensively employed in various configurations for the detection of chemical and biological analytes, owing to their rapid response, high sensitivity, and reliable performance [1], [2]. Among the different configurations, the Kretschmann configuration utilizing a prism as the coupling medium has been the most commonly used for SPR based sensor applications [2]. Notably, fiber-optic SPR sensors offer significant advantages, including immunity to electromagnetic interference, suitability for remote sensing, miniaturization and high resistance to corrosive environments. However, the conventional optical fiber-based sensors require removal of the cladding in order to increase the proximity of metal dielectric interface to the core thereby enhancing the performance of the sensor [3], [4]. Apart from conventional fibers, photonic crystal fibers based on various geometrical configurations have also been reported for SPR based sensing applications [5], [6], [7], [8], [9], [10], [11], [12]. Most of the PCF based configurations especially those involve small holes of different diameters are complex and difficult to fabricate [6], [7]. Additionally, the metal coatings have been used either on polished PCF or on the inner surface of the holes of PCF [8], [9], [10], [11], [12]. However, physical polishing may lead to the formation of very rough or non-uniform surface while the chemical polishing may be time consuming. Furthermore, the removal of analyte from small holes of PCF will be difficult owing to the higher adhesive force between the wall of capillary and the liquid in comparison to the cohesive force. Therefore, a fiber with large air hole and a core directly exposed to the air hole would be a more effective configuration for SPR-based applications.

All the above-described sensors are mostly based on the silica fibers which are fragile after the removal of coating. While silica-based fiber sensors are capable of detecting various chemical parameters using SPR technique, their relatively high Young's modulus (∼70 GPa) poses limitations

The associate editor coordinating the review of this manuscript and approving it for publication was David Caplan.

for applications that involve tight spaces with small bending radii e.g detection in internal parts of the body [13]. However, polymer fibers due to their unique properties such as larger elastic strain limit, low Young's modulus, low brittleness, enhanced bending tolerance and biocompatibility can be used to address the fragileness of silica fibers [13]. Over the few decades, progress has been achieved in the fabrication of various types of polymer fibers such as PMMA, TOPAS, and CYTOP [14], [15], [16]. However, the humidity sensitivity and use of dopants in PMMA makes their applications limited [14]. On the other hand, the chemical inertness and humidity insensitivity of cyclic olefin copolymers-based fibers, such as Topas, CYTOP, and ZEONEX make them an attractive choice for sensing applications [15], [16], [17]. Among these ZEONEX has edge over other polymers owing to the availability of different grades of ZEONEX that can be used for the fabrication of core and cladding without the requirement of any dopant. This not only helps in avoiding the possibility of dopant diffusion during the drawing of the optical fiber but also makes the drawing process easier due to the similar glass transition temperature of the core and cladding materials [18].

Most of the proposed fibers based on ZEONEX have been investigated for applications in terahertz regime [19], [20], [21], [22], [23]. For example, air hole based single mode ZEONEX fiber have been fabricated and characterized for terahertz regime [19]. Additionally, a number of microstructured PCF and porous fibers based on ZEONEX have been proposed and numerically analyzed [20], [21], [22], [23]. For example, a hexagonal shaped PCF have been proposed for the detection of tuberculosis [20]. A diamond shaped Kagome lattice and a sloted core PCF have been proposed for terahertz waveguiding [21], [23]. A dual channel SPR based sensor have been proposed for gaseous analytes in terahertz regime using porous fiber [24]. However, during the drawing of polymer fiber the small air holes usually collapse and it will be challenging to fabricate most of the above reported fibers for practical applications. In addition to the application in terahertz regime, ZEONEX based fibers have also been fabricated and demonstrated for strain sensing applications in visible and near IR region [25], [26]. As discussed above, a very few investigations have been conducted for ZEONEX based fibers for surface plasmon based sensor applications [24].

In this paper we present a numerical analysis of a fabricated ZEONEX based large single air hole assisted optical fiber for SPR sensing applications in visible wavelength region where the transmission loss for ZEONEX is less. The fiber can be easily fabricated using pull through technique and the large air hole assist in easier removal of analyte from the fiber. The inner surface of the large air hole has been coated with gold and the core has been exposed to the air hole. The thickness of the gold layer has been optimized. The sensitivity of the proposed fiber sensor has been analyzed with respect to variations in both the refractive index (RI) and

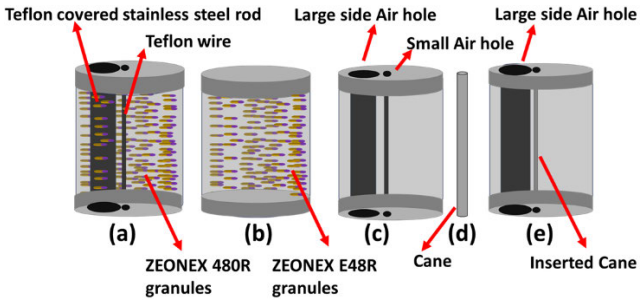

FIGURE 1. (a) shows a teflon covered stainless steel rod and a teflon wire passing through a glass cylinder filled with ZEONEX 480R granules. (b) shows a glass cylinder filled with ZEONEX E48R.(c) shows the preform for cladding of LSAHPOF.(d) refers to the cane drawn out of melted granules shown in (b). (e) corresponds to the final preform fabricated by inserting the cane shown on (d) into the cladding preform shown in (c).

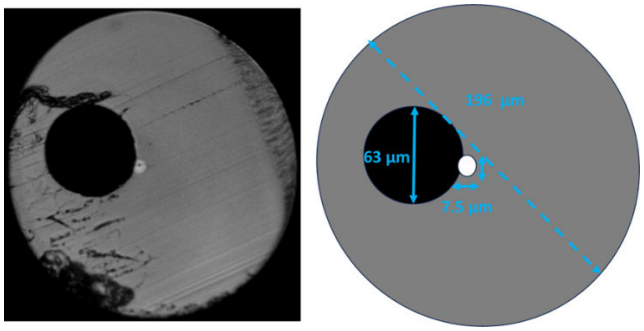

FIGURE 2. (a) shows the cross-section of the fabricated LSAHPOF illuminated with white light and (b) shows the corresponding schematic of the fiber considered for numerical analysis.

the biolayer thickness. A maximum wavelength sensitivity of 3500 nm/RIU and a maximum amplitude sensitivity of 696 RIU^{-1} have been achieved. The effect of diameter of the air hole on the performance of the senor has been analyzed. Additionally, the sensor demonstrates a biolayer thickness sensitivity of 1.54, with a corresponding resolution of 64 pm.

II. FABRICATION OF LSAHPOF

The LSAHPOF was fabricated from a preform comprising a cladding and a core. The cladding preform was prepared using a glass tube sealed at one end with a Teflon cap. This cap featured a large side hole and a small hole positioned close (approximately 200–300 μm) to it as illustrated in Figure. 1(a). A teflon-coated stainless steel rod was inserted through the side hole, while a teflon wire was inserted through the small hole. The glass tube was then filled with ZEONEX 480R polymer granules and sealed at the opposite end with a second Teflon cap of identical geometry, as depicted in Figure 1(a). Separately, a second glass tube intended for the core preform was sealed at one end and filled with ZEONEX E48R granules, as shown in Figure 1(b). It is to be noted that both kinds of ZEONEX granules have different refractive indices with ZEONEX E48R having higher RI than ZEONEX 480R. The glass tubes meant for cladding and core preform were heated at 250 °C for 20 hours to melt

the polymer granules and facilitate the removal of trapped oxygen and air. This was followed by a controlled cooling process lasting 10 hours. Following the heat treatment, the stainless-steel rod and teflon wire were carefully removed from the cladding preform, resulting in the formation a side hole and a smaller adjacent hole as illustrated in Figure 1(c). The resulting core preform was subsequently drawn into a cane with a diameter of 0.9 mm also shown in Figure 1(d). This cane was then inserted into the central hole of the cladding preform as illustrated in Figure1(e). The assembled structure was finally drawn into an optical fiber using pull through technique as depicted in Figure 2 [27]. It is to be noted that in contrast to the previous work, in this case the core touches the air hole. This can be accomplished by keeping the air hole close to the core during the fabrication of preform and carefully tuning the air pressure during the drawing process. The elliptical structure of core and cladding can be attributed to the asymmetric position of the air hole that affects the shape of the fiber during the drawing process. The reported structure is reproducible, with only slight variations in the fiber diameter across different sections, which in turn leads to minor variations in the air-hole and core diameters.

III. THEORETICAL MODELLING

The cross section of the LSAHPOF is shown in Figure 2(a). The schematic of the fabricated structure that has been considered for numerical simulation is illustrated in Figure 2(b). The diameter of the fiber is 196 μm. The core is slightly elliptical and the length of its major and minor axis are 7.5 and 8.5 μm respectively. The diameter of the large air hole is 63 micrometer. It is to be noted here that the shape of outer portion of the cladding does not affect the performance of the SPR sensor. ZEONEX exhibits a low propagation loss of approximately 3–4 dB/m within the 400–700 nm wavelength range, with the loss increasing exponentially beyond 850 nm [26]. However, the sensor can still be operated beyond 850 nm since the probe length is typically only a few centimeters and the loss beyond this wavelength would not significantly affect the overall sensor performance [18]. In this work, gold has been selected as the plasmonic material due to its ability to support surface plasmon resonance within the visible spectrum. Therefore, a coating of a uniform layer of gold is considered along the inner surface of the circular air hole. Among the coated region, only a localized segment measuring 6.4 μm in length serves as the active interaction zone due to its proximity to the core. The coating of gold layer can be accomplished using physical vapor deposition technique. The refractive index of ZEONEX has been considered from the ellipsometry data with a fitting curve [17]. The dielectric constant of gold has been determined following the Drude–Lorentz model [28].

$$\varepsilon_m(\lambda) = 1 - \frac{\lambda^2 \lambda_c}{\lambda_p^2(\lambda_c + i\lambda)} \tag{1}$$

Where λ_c and λ_p refer to the collision and plasma wavelength of gold respectively and λ_c =8.9342 μm and λ_p =0.16826 μm. The modal propagation characteristics of the proposed LSAHPOF were investigated using a finite element method (FEM)-based computational analysis tool (COMSOL). The entire cross section of the fiber is divided into a large number of finite triangular elements with the number of domain elements being 56909. The propagation of light is considered along z direction while the cross section lies in XY plane. The sensor's performance is assessed by evaluating the confinement loss of the fundamental core mode, resulting from resonant coupling between the guided mode and surface plasmon polaritons at the metal–dielectric interface. The loss could be defined as [29]

$$Loss = 8.686 \times \left(\frac{2\pi}{\lambda}\right) Im\left(n_{eff}\right) \times 10^4 dB/cm \tag{2}$$

Furthermore, the sensitivity of the proposed sensor can be investigated through two distinct interrogation mechanisms, namely amplitude interrogation and wavelength interrogation, each offering unique advantages in detecting refractive index variations. In amplitude interrogation, the intensity of the output beam is monitored at a fixed wavelength, eliminating the need for spectral scanning. Consequently, this approach requires only a power meter, making it more cost-effective. However, this interrogation method has a narrower operational range compared to wavelength-based interrogation. Additionally, the sensor performance is susceptible to fluctuations in the source power, which can affect measurement accuracy. In contrast, wavelength interrogation is insensitive to transmission losses and offers a broader operational range, providing higher measurement accuracy and robustness. The wavelength sensitivity of the sensor can be defined as [29]

$$S_\lambda\ (nm/RIU) = \frac{\Delta\lambda_{res}}{\Delta n_a} \tag{3}$$

where the numerator and the denominator on the right side refers to the change in resonance wavelength and change in RI of analyte respectively. On the other hand, the amplitude sensitivity can be defined as [29]

$$S_A(\lambda)\left(RIU^{-1}\right) = -(\partial\alpha(\lambda, n_a)/\partial n_a)/\alpha(\lambda, n_a) \tag{4}$$

The wavelength sensitivity for change in thickness of bio-layer (T_b) is defined as

$$S = d\lambda_{peak}/dT_b \tag{5}$$

IV. PROPOSED EXPERIMENTAL SET UP

The proposed structure is suitable for sensing applications using a reflection-based experimental setup, as illustrated in Figure.3. Light from a broadband white light source can be coupled into one input arm of a 2 × 1 optical coupler, while the other input/output arm can be connected to a spectrometer for monitoring the reflected signal. The common output port of the coupler can be butt-coupled to a short segment of LSAHPOF. The Fresnel reflection at the interface

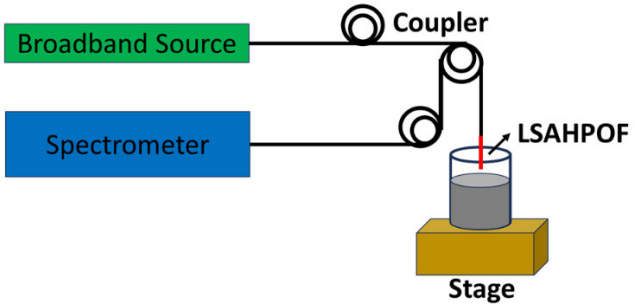

FIGURE 3. Schematic of the proposed experimental set up for the detection of RI of analyte and thickness of biolayer.

between the silica-based single-mode fiber and the polymer fiber can be minimized using a drop of index-matching glue. During the butt-coupling process, the reflected optical power could be continuously monitored via the spectrometer. Once the reflected power is maximized—indicating optimal alignment—the interface between the single-mode or multimode fiber and the LSAHPOF can be fixed using optical-grade adhesive, and mechanically protected with a suitable sleeve. For refractive index (RI) sensing, the tip of the LSAHPOF segment can be immersed in the target solution, allowing the reflected signal to vary with the RI of surrounding medium.

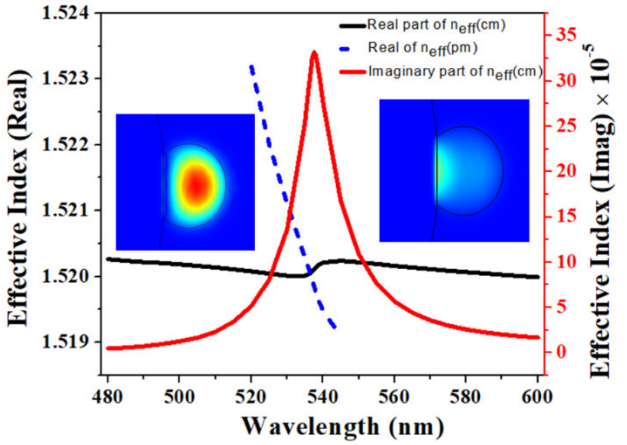

FIGURE 4. Variation in real part of effective index of core mode (black solid line) and plasmonic mode (blue doted line) and imaginary part of effective index of core mode (red solid line) with wavelength.

V. RESULTS AND DISCUSSIONS

Both X- and Y-polarized modes can propagate through the core of LSAHPOF, the X-polarized mode is specifically analyzed. The larger side hole is aligned along the X-axis, and its inner wall is coated with gold. Consequently, the interaction of the X-polarized mode is dominant, since along the Y-axis there is no metal coating and hence no dielectric–metal interface to support surface plasmon excitation. It should also be noted that, in the simulation, the line connecting the fiber core center and the side hole is defined along the X-axis. The interaction of the X polarized mode with the gold analyte interface leads to the excitation of the surface plasmon mode which in turn will lead to the propagation loss of the core mode. The confinement loss of the core mode is directly related to the imaginary part of its complex effective refractive index and can be expressed as equation (2). The dispersion curve for core mode and plasmonic mode is depicted in Figure.4. The intersection of the dispersion curves for the core mode and the surface plasmon polariton (SPP) mode signifies phase-matching between the two modes, thereby enabling efficient power transfer. This coupling mechanism manifests into a pronounced peak in the imaginary component of the effective index of the core mode which directly corresponds to the point of maximum confinement loss as defined in equation (4). The insets in Figure.4 shows the mode profile of core mode, coupled mode and the plasmonic mode.

The confinement loss depends on the geometry and the thickness of the metal layer. However, the simpler geometry of the proposed structure leads to the requirement for optimization of only thickness of gold. In this case, the thickness of gold has been varied from 30 to 50 nm and the corresponding confinement loss is shown in Figure.5. As can be seen from the figure, the loss gradually decreases with thickness and the peak wavelength corresponding to maximum loss shows red shift. The lower thickness of gold will lead to better interaction of surface plasmon wave with the analyte. Furthermore, higher thickness leads to the shift of resonance wavelength to higher wavelength region where the propagation loss of ZEONEX will be more. Therefore, further analysis of the performance of the proposed structured is carried out considering the thickness of gold as 30 nm.

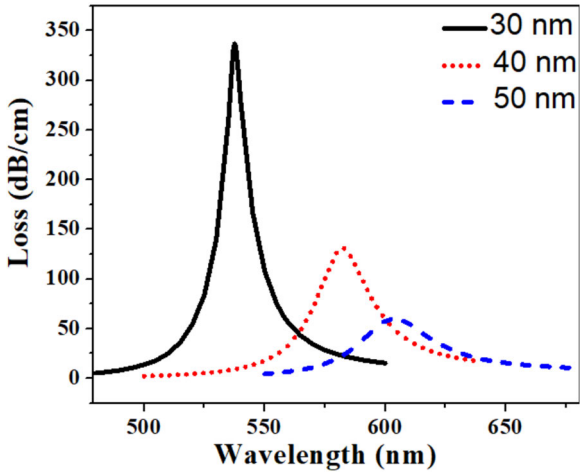

FIGURE 5. Variation in confinement loss of core mode with thickness of gold.

AS depicted in Figure 3, the proposed structure can be immersed in the analyte thereby filling the air hole with the analyte medium. Any real-time change in the analyte's refractive index (RI) leads to a corresponding shift in the resonance peak wavelength due to modification of the effective refractive index of the surrounding medium. In this study, the RI of the analyte was varied from 1.40 to 1.44, and the

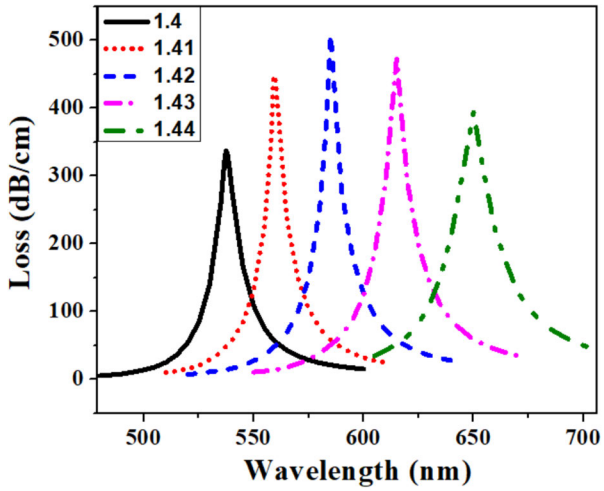

FIGURE 6. Variation in confinement loss with change in RI of analyte.

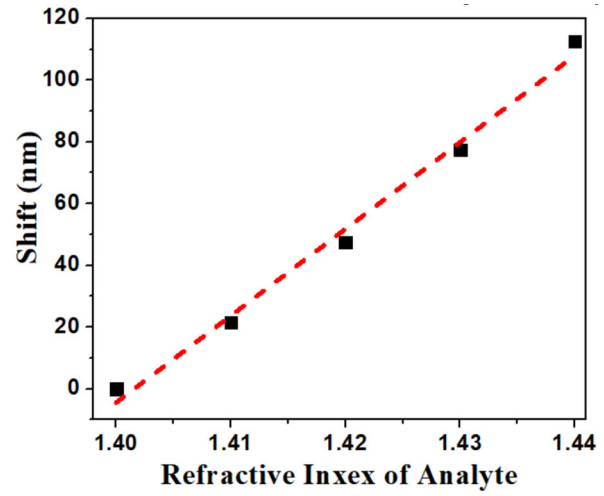

FIGURE 7. Shift in resonance peak wavelength with change in RI of analyte.

resulting shifts in the resonance spectrum are illustrated in Figure 6. As observed, the resonance peak exhibits a redshift from 537.5 nm to 559 nm as the RI increases from 140 to 141 thereby resulting in a sensitivity of 2100 nm/RIU The sensitivity continues to increase with increase in RI of analyte, reaching 3500 nm/RIU for a change from 1.43 to 1.44. This shift arises from the alteration in phase-matching conditions between the core-guided mode and the surface plasmon resonance mode induced by the RI change. The linear relationship between the resonance wavelength shift and the analyte RI is depicted in Figure. 7. Furthermore, considering a spectrometer resolution of 0.1 nm, the refractive index (RI) resolution of the proposed sensor is calculated to be 5×10^{-5} RIU. This resolution improves to 2.8×10^{-5} RIU for analytes with higher refractive indices, specifically for a change in RI from 1.43 to 1.44. Table-1 presents the results obtained from the proposed probe along with a comparison to recently reported polymer fiber–based SPR sensors [24], [30], [31], [32], [33], [34]. The proposed polymer fiber is generally

TABLE 1. Sensitivities of polymer fiber based SPR sensors.

Polymer fiber	Wavelength Regime	Sensitivity	Reference
ZEONEX	IR-Microwave	1,10000 nm/RIU	[24]
PMMA	Visible	2258 nm/RIU	[30]
PMMA	Visible	4284.8 nm/RIU	[31]
Tapered PMMA fiber	Visible	1700nm/RIU	[32]
PMMA	Visible	12.5 dB/RIU	[33]
PMMA	Visible	1570nm/RIU	[34]
Our work	Visible	3500 nm/RIU	

sensitive to temperature variations and the typical temperature sensitivity is around 10 pm/°C [13], [26]. An FBG can be inscribed in the core to enable simultaneous measurement of the analyte's refractive index and temperature, thereby compensating for errors arising from temperature fluctuations.

In the above discussion the diameter of the air hole was considered to be 63 μm. In order to verify the performance of the proposed structure for large air hole, the diameter of air hole is increased to 100 μm. However, during the drawing process, when the diameter of air hole is increased, the corresponding total diameter and the core diameter is increased accordingly. Therefore, the new total diameter of fiber becomes 312 μm and the length of semimajor and semi minor axis of the core becomes 13.5 μm and 12 μm respectively. The performance of this fiber is analyzed by considering two analytes with refractive index of 1.4 and 1.41 and the corresponding shift in resonance spectrum is shown in Figure 8. As can be seen from the figure, the peak shifts from 539 nm to 560.5 nm resulting in a total shift of 21.5 nm. On the other hand, for the same change in refractive index, the shift for the LSAHPOF with air hole diameter of 63 μm was also 21.5 nm. It is to be noted that the sensitivity generally depends on the effective indices of the core mode and the plasmonic mode, as well as on the metal thickness. When the air-hole diameter is increased from 63 to 100 μm (with a corresponding increase in the core diameter), the effective indices of both the core mode and the plasmonic mode exhibit only negligible variation. As a result, the resonance wavelength exhibits only a slight shift, from 537.5 nm (for diameter = 63 μm) to 539 nm (for diameter = 100 μm) when the analyte refractive index is 1.40. Upon changing the analyte refractive index to 1.41, the resonance peak shifts accordingly, while the net wavelength shift remains essentially unchanged. This confirms the performance of sensor remains same even if the diameter of fiber is increased thereby making it more suitable for light coupling as well as deposition of metal and other biomolecules.

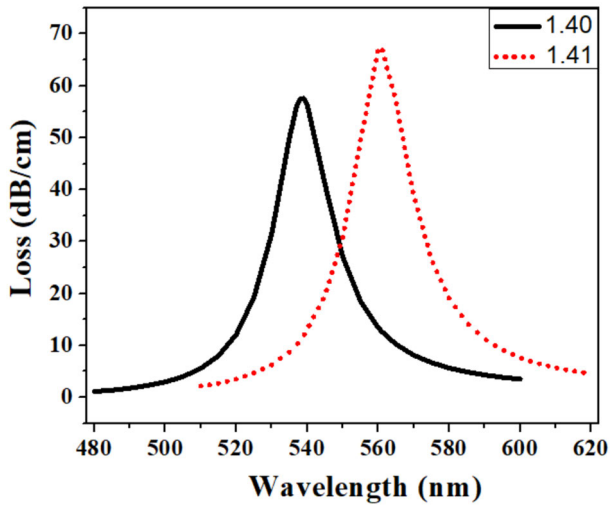

FIGURE 8. Shift in resonance peak wavelength corresponding to the confinement loss in core mode for LSAHPOF with an air hole of diameter 100μm.

The interrogation scheme is also extended to detection of change in amplitude at a particular wavelength. When the refractive index (RI) of the analyte is varied from 1.40 to 1.41, the amplitude sensitivity of the proposed sensor reaches 696 RIU^{-1} at a wavelength of 560 nm, as illustrated in Figure 9. Assuming the detector can resolve a 1% change in intensity, the corresponding sensor resolution is calculated to be 1.4×10^{-5} RIU.

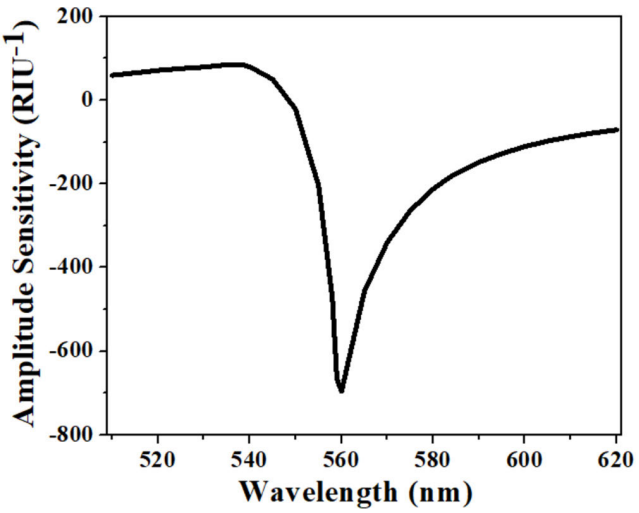

FIGURE 9. Variation in amplitude sensitivity with wavelength.

The preceding analysis demonstrates the sensor's effectiveness in detecting the refractive index (RI) of the analyte, and this sensing principle can be extended to monitor variations in biolayer thickness. For typical biosensing applications, the metal surface is usually coated with a thin biolayer, which typically has a RI in the range of 1.4 to 1.42. This biolayer, composed of biomolecules such as antibodies, activates the

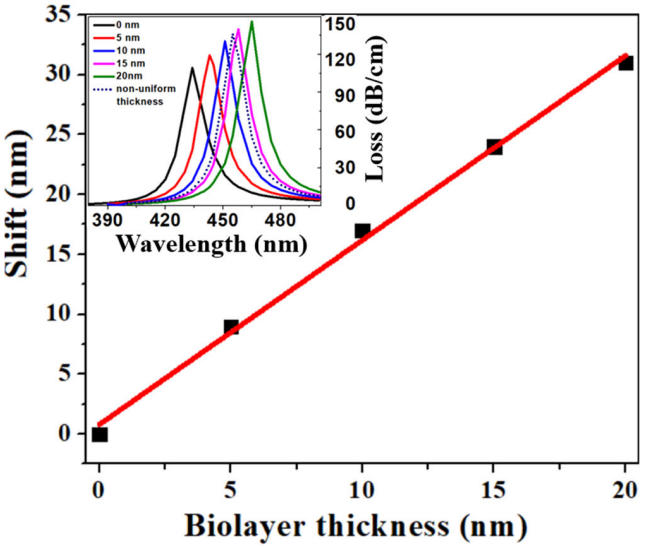

FIGURE 10. The shift in peak resonance wavelength with biolayer thickness for a biolayer refractive index of 1.410. The inset shows the corresponding change in confinement loss of the fundamental core mode with wavelength. The dotted curve in the inset corresponds to biolayer of non-uniform thickness.

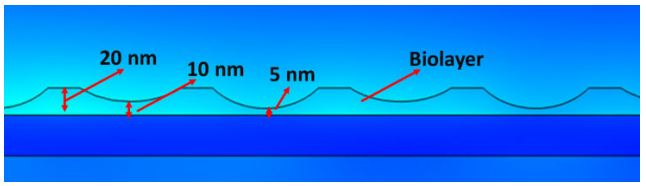

FIGURE 11. The shift in peak resonance wavelength with biolayer thickness for a biolayer refractive index of 1.410. The inset shows the corresponding change in confinement loss of the fundamental core mode with wavelength.

metal surface to enable specific detection of target protein molecules through a lock-and-key binding mechanism. The thickness of the deposited biolayer can be quantified by monitoring the shift in the surface. Once the biolayer thickness is characterized, the subsequent binding of specific proteins to the immobilized antibodies can also be tracked through additional resonance shifts. In our analysis, we considered a biolayer with a refractive index of 1.410, while the external medium above the biolayer was assumed to be aqueous, with an RI of 1.33. The biolayer thickness was varied from 0 to 20 nm, and the corresponding shifts in the resonance wavelength are illustrated in Figure 10, which demonstrates a sensitivity of 1.54. The inset of the figure shows the resonance spectrum shift. In the above simulations, we have considered a biolayer with uniform thickness. Such uniformity causes a consistent resonance shift across the interface. However, in the case of a non-uniform biolayer, the effective index varies across different regions of the metal–dielectric interface, leading to slightly different resonance wavelengths in each region. In order to simulate the performance of the sensor for a non-uniform biolayer, the thickness was varied across the metal surface, with a minimum of 5 nm and a maximum of 20 nm, as shown in Figure 11. The resulting

shift in the resonance peak was found to be 21 nm. Considering the slope of 1.54 calculated above, a resonance shift of 21 nm corresponds to an effective average biolayer thickness of 13.6 nm. Hence, for a biolayer with non-uniform thickness, the average thickness value can be estimated using this approach. Considering a spectrometer resolution of 0.1 nm, a detection resolution of approximately 64 picometers (pm) is achievable.

VI. CONCLUSION

A ZEONEX-based polymer optical fiber (POF) incorporated with a large side air hole has been proposed and numerically analyzed for refractive index (RI) sensing and thickness of biolayer detection using surface plasmon resonance (SPR). ZEONEX granules were utilized to fabricate the preform, and the fiber was subsequently drawn using the pull-through technique. During the fiber drawing process, the internal pressure was carefully optimized to allow the fiber core to come into contact with an adjacent side air hole. The sensors performance has been analysed over a refractive index range of 1.40 to 1.44, which corresponds to the typical refractive indices of many biomolecules. Numerical analysis showed that the sensor has wavelength sensitivity of 3500 nm/RIU and an amplitude sensitivity of 696 RIU^{-1}. For wavelength-based interrogation, the maximum achievable resolution is estimated to be 2.8×10^{-5} RIU. Furthermore, the sensor demonstrates a sensitivity of 1.54 to changes in biolayer thickness, with a minimum detection resolution of 64 picometers. For a biolayer of non-uniform thickness, the sensor predicted average value of thickness. Therefore, due to its compact architecture, the proposed fiber structure is well-suited for miniaturized biosensing applications, where a small fiber tip is sufficient to detect refractive index changes using a reflection-based experimental setup.

ACKNOWLEDGMENT

The authors are thankful to Dr. Getinet Woyessa (DTU Electro) for providing the ellipsometry data for the dispersion of ZEONEX (480R and E48R). They are thankful to Dr. S. Selvendran (CHAIR, VIT Chennai) for COMSOL support.

REFERENCES

[1] E. Kretschmann and H. Raether, "Radiative decay of nonradiative surface plasmons excited by light," *Zeitschrift für Naturforschung A*, vol. 23, no. 12, pp. 2135–2136, Dec. 1968.

[2] J. Homola, S. S. Yee, and G. Gauglitz, "Surface plasmon resonance sensors: Review," *Sens. Actuators B, Chem.*, vol. 54, no. 1, p. 3, Jan. 1999.

[3] Y. Zhou and X. Yan, "D-shaped fiber surface plasmon resonance refractive index sensor enhanced by MXene (Ti3C2Tx)," *IEEE Photon. J.*, vol. 14, no. 5, pp. 1–7, Oct. 2022.

[4] W. Lin, O. Bang, and G. Woyessa, "Mid-infrared surface plasmon resonance fiber optic sensors," *Opt. Exp.*, vol. 33, no. 2, pp. 1962–1968, Jan. 2025.

[5] D. J. J. Hu and H. P. Ho, "Recent advances in plasmonic photonic crystal fibers: Design, fabrication and applications," *Adv. Opt. Photon.*, vol. 9, no. 2, pp. 257–314, Jun. 2017.

[6] J. He, J. Wang, L. Yang, J. Lv, W. Liu, Q. Liu, P. K. Chu, and C. Liu, "Ring-core photonic crystal fiber sensor based on SPR for extra-wide refractive index detection," *Coatings*, vol. 13, no. 7, p. 1207, Jul. 2023.

[7] M. M. Rahman, M. M. Rana, M. S. Anower, M. S. Rahman, and A. K. Paul, "Design and analysis of photonic crystal fiber-based plasmonic microbiosensor: An external sensing scheme," *Social Netw. Appl. Sci.*, vol. 2, no. 7, Jul. 2020, Art. no. Article 1194.

[8] X. Luo, W. Liu, J. Lv, L. Yang, J. Wang, P. K. Chu, and C. Liu, "High-sensitivity dual U-shaped PCF-SPR refractive index sensor for the detection of gas and liquid analytes," *J. Opt. Soc. Amer. A, Opt. Image Sci.*, vol. 41, no. 4, pp. 595–605, Apr. 2024.

[9] S. Gao, K. Wei, H. Yang, Y. Tang, Z. Yi, C. Tang, B. Tang, Y. Yi, and P. Wu, "Design of surface plasmon resonance-based D-type double open-loop channels PCF for temperature sensing," *Sensors*, vol. 23, no. 17, p. 7569, 2023.

[10] S. Ullah, H. Chen, P. Guo, M. Song, S. Zhang, L. Hu, and S. Li, "A highly sensitive D-shaped PCF-SPR sensor for refractive index and temperature detection," *Sensors*, vol. 24, no. 17, p. 5582, Aug. 2024.

[11] W. Qin, S. Li, Y. Yao, X. Xin, and J. Xue, "Analyte-filled core self-calibration microstructured optical fiber based plasmonic sensor for detecting high refractive index aqueous analyte," *Opt. Lasers Eng.*, vol. 58, pp. 1–8, Jul. 2014.

[12] A. Hassani and M. Skorobogatiy, "Design of the microstructured optical fiber-based surface plasmon resonance sensors with enhanced microfluidics," *Opt. Exp.*, vol. 14, no. 24, p. 11616, 2006.

[13] J. N. Dash, X. Cheng, D. S. Gunawardena, and H.-Y. Tam, "Rectangular single-mode polymer optical fiber for femtosecond laser inscription of FBGs," *Photon. Res.*, vol. 9, no. 10, p. 1931, Oct. 2021.

[14] I.-L. Bundalo, R. Lwin, S. Leon-Saval, and A. Argyros, "All-plastic fiber-based pressure sensor," *Appl. Opt.*, vol. 55, no. 4, pp. 811–816, Feb. 2016.

[15] G. Emiliyanov, J. B. Jensen, O. Bang, P. E. Hoiby, L. H. Pedersen, E. M. Kjær, and L. Lindvold, "Localized biosensing with topas microstructured polymer optical fiber," *Opt. Lett.*, vol. 32, no. 5, pp. 460–462, Mar. 2007.

[16] A. G. Leal-Junior, A. Theodosiou, C. A. R. Diaz, L. M. Avellar, K. Kalli, C. Marques, and A. Frizera, "FPI-POFBG angular movement sensor inscribed in CYTOP fibers with dynamic angle compensator," *IEEE Sensors J.*, vol. 20, no. 11, pp. 5962–5969, Jun. 2020.

[17] P. Akrami, A. I. Adamu, G. Woyessa, H. K. Rasmussen, O. Bang, and C. Markos, "All-polymer multimaterial optical fiber fabrication for high temperature applications," *Opt. Mater. Exp.*, vol. 11, no. 2, pp. 345–354, Feb. 2021.

[18] J. Narayan Dash, J. Cui, X. Cheng, and H.-Y. Tam, "Miniature accelerometer based on rectangular multicore polymer optical fiber and fs-laser inscribed fiber fan-out device," *Opt. Laser Technol.*, vol. 180, Jan. 2025, Art. no. 111476.

[19] J. Anthony, R. Leonhardt, A. Argyros, and M. C. J. Large, "Characterization of a microstructured Zeonex terahertz fiber," *J. Opt. Soc. Amer. B, Opt. Phys.*, vol. 28, no. 5, p. 1013, May 2011.

[20] R. Hossen, M. S. Hossain, S. A. Mim, M. Al-Amin, S. Ahmed, M. Ashrafuzzaman, M. A. Salahin, and S. Sen, "Design of hexagonal shaped spectroscopy based biosensor for the detection of tuberculosis," *Sens. Bio-Sensing Res.*, vol. 45, Aug. 2024, Art. no. 100682.

[21] J. Sultana, M. R. Islam, M. Faisal, K. M. Abu Talha, and M. S. Islam, "Design and analysis of a Zeonex based diamond-shaped core Kagome lattice photonic crystal fiber for T-ray wave transmission," *Opt. Fiber Technol.*, vol. 47, pp. 55–60, Jan. 2019.

[22] M. S. Islam, J. Sultana, A. Dinovitser, B. W.-H. Ng, and D. Abbott, "A novel Zeonex based oligoporous-core photonic crystal fiber for polarization preserving terahertz applications," *Opt. Commun.*, vol. 413, pp. 242–248, Apr. 2018.

[23] N. I. B. Hamid, M. R. Islam, M. R. H. Khan, K. M. A. Talha, and A. N. M. Iftekher, "High birefringent slotted core slotted cladding porous core PCF for THz waveguide," *Opt. Commun.*, vol. 574, Jan. 2025, Art. no. 131120.

[24] G. Liu, F. Tian, Y. Lu, Z. Han, C. Yao, B. Wang, Y. Zhang, L. Li, and J. Zhang, "Zeonex-based high sensitivity dual-channel SPR optical fiber sensor for gaseous analytes in terahertz regime," *Optik*, vol. 255, Apr. 2022, Art. no. 168656.

[25] R. Oliveira, L. Bilro, T. H. R. Marques, C. M. B. Cordeiro, and R. Nogueira, "Strain sensitivity enhancement of a sensing head based on ZEONEX polymer FBG in series with silica fiber," *J. Lightw. Technol.*, vol. 36, no. 22, pp. 5106–5112, Nov. 15, 2018.

[26] G. Woyessa, H. K. Rasmussen, and O. Bang, "Zeonex—A route towards low loss humidity insensitive single-mode step-index polymer optical fibre," *Opt. Fiber Technol.*, vol. 57, Jul. 2020, Art. no. 102231.

[27] J. N. Dash, X. Cheng, and H. Tam, "Low gas pressure sensor based on a polymer optical fiber grating," *Opt. Lett.*, vol. 46, no. 5, pp. 933–936, Mar. 2021.
[28] P. K. Maharana, T. Srivastava, and R. Jha, "Low index dielectric mediated surface plasmon resonance sensor based on graphene for near infrared measurements," *J. Phys. D, Appl. Phys.*, vol. 47, no. 38, Sep. 2014, Art. no. 385102.
[29] J. N. Dash, R. Das, and R. Jha, "AZO coated microchannel incorporated PCF-based SPR sensor: A numerical analysis," *IEEE Photon. Technol. Lett.*, vol. 30, no. 11, pp. 1032–1035, Jun. 1, 2018.
[30] G. Woyessa and O. Bang, "Sensitivity enhancement of polymer optical fiber surface plasmon resonance sensor utilizing ITO overlayer," *Sensors*, vol. 25, no. 6, p. 1863, Mar. 2025.
[31] L. Liu, S. Deng, J. Zheng, L. Yuan, H. Deng, and C. Teng, "An enhanced plastic optical fiber-based surface plasmon resonance sensor with a double-sided polished structure," *Sensors*, vol. 21, no. 4, p. 1516, Feb. 2021.
[32] N. Cennamo, F. Arcadio, A. Minardo, D. Montemurro, and L. Zeni, "Experimental characterization of plasmonic sensors based on lab-built tapered plastic optical fibers," *Appl. Sci.*, vol. 10, no. 12, p. 4389, Jun. 2020.
[33] Y. Hu, Y. Hou, A. Ghaffar, and W. Liu, "A narrow groove structure based plasmonic refractive index sensor," *IEEE Access*, vol. 8, pp. 97289–97295, 2020.
[34] N. Jing, J. Zhou, K. Li, Z. Wang, J. Zheng, and P. Xue, "Refractive index sensing based on a side-polished macrobend plastic optical fiber combining surface plasmon resonance and macrobending loss," *IEEE Sensors J.*, vol. 19, no. 14, pp. 5665–5669, Jul. 2019.

JITENDRA NARAYAN DASH received the M.Tech. degree in laser and electro-optical engineering from Anna University, Chennai, India, in 2010, and the Ph.D. degree from the Nanophotonics and Plasmonics Laboratory, School of Basic Sciences, IIT Bhubaneswar, India, in 2017. He was a Visiting Student at the Raman Research Institute, Bengaluru, India, from 2010 to 2011. He was a Research Associate at The Hong Kong Polytechnic University, from 2018 to 2022, where he was a Research Fellow, from 2022 to 2023. Currently, he is an Assistant Professor (Senior Grade) with VIT Chennai. He has authored and co-authored over 35 peer-reviewed research articles in internationally reputed journals. He was awarded the National Post-Doctoral Fellowship by the Science and Engineering Research Board, Government of India, from 2017 to 2018, while conducting research at NISER Bhubaneswar.

CHENG XIN received the M.S. degree from Northeast Normal University, Changchun, China, in 2009, and the Ph.D. degree from Jinan University, Guangzhou, China, in 2019. In 2009, he joined the Photonic Research Center, The Hong Kong Polytechnic University (PolyU PRC), as a Research Assistant, where he was a Postdoctoral Research Fellow, in 2019. He is currently a Scientific Officer with PolyU PRC. His research interests mainly include specialty optical fiber design on materials, fabrication technology, and sensing devices, including physical parameters, chemical quantities, and biomedical areas.

HWA-YAW TAM (Life Fellow, IEEE) received the B.Sc. and Ph.D. degrees in electrical and electronic engineering from The University of Manchester, Manchester, U.K., in 1985 and 1990, respectively. From 1989 to 1993, he was with the Hirst Research Centre, GEC-Marconi Ltd., London, U.K., working on optical components, WDM systems, erbium optical fiber amplifiers, and fiber lasers. He is currently the Chair Professor of photonics, the former Head of the Electrical Engineering Department, and the Associate Director of the Photonic Research Institute, The Hong Kong Polytechnic University, Hong Kong. He has authored or co-authored over 700 technical articles, holds 14 patents, and has an H-index of 66 in Google Scholar. He has developed and installed optical fiber sensing systems for condition and predictive maintenance of railways in Hong Kong, China, Mainland, Taiwan, Singapore, The Netherlands, Australia, and India. His current research interests include the design and fabrication of specialty optical fibers for sensor applications and optical monitoring systems related to railways, smart buildings, batteries, and medical devices. He is an Optica Fellow. He was the Winner of the Prestigious 2014 Berthold Leibinger Innovationspreis Prize for his laser sensing technology contribution in railway monitoring.